

Kirigami-Inspired Self-Assembly of 3D Structures

Arif M. Abdullah,* Xiuling Li, Paul V. Braun, John A. Rogers, and K. Jimmy Hsia*

Self-assembly of 3D structures presents an attractive and scalable route to realize reconfigurable and functionally capable mesoscale devices without human intervention. A common approach for achieving this is to utilize stimuli-responsive folding of hinged structures, which requires the integration of different materials and/or geometric arrangements along the hinges. It is demonstrated that the inclusion of Kirigami cuts in planar, hingeless bilayer thin sheets can be used to produce complex 3D shapes in an on-demand manner. Nonlinear finite element models are developed to elucidate the mechanics of shape morphing in bilayer thin sheets and verify the predictions through swelling experiments of planar, millimeter-scaled PDMS (polydimethylsiloxane) bilayers in organic solvents. Building upon the mechanistic understandings, the transformation of Kirigami-cut simple bilayers into 3D shapes such as letters from the Roman alphabet (to make “ADVANCED FUNCTIONAL MATERIALS”) and open/closed polyhedral architectures is experimentally demonstrated. A possible application of the bilayers as tether-less optical metamaterials with dynamically tunable light transmission and reflection behaviors is also shown. As the proposed mechanistic design principles could be applied to a variety of materials, this research broadly contributes toward the development of smart, tetherless, and reconfigurable multifunctional systems.

synthesis) to a few millimeters (too small for traditional top-down machining techniques).^[1] Although it is possible to achieve millimeter-scaled structures through additive manufacturing such as high-resolution 3D printing techniques, those processes are limited by material compatibility, nozzle design, and speed. As the opportunity of human intervention is minimal at these length-scales, the final structure must be self-assembled through the interactions between individual components.^[1,2] A particular example is the generation of complex proteins where, individual amino acids spontaneously bond together in a way that leads to 3D folded shapes responsible for the protein's structure and hence, functionalities.^[3] This type of self-generated behavior (also known as self-folding^[4,5]) is also observed in diverse classes of natural systems across length scales such as the shape transformation of plants (through differential turgor in response to environmental changes),^[6,7] wrinkling of apple skins (arising from the drying of underlying flesh),^[8] and gyrification of mamma-

1. Introduction

Freestanding functional systems with complex 3D architectures become difficult to fabricate when the characteristic length scale is between micrometers (too big for bottom-up chemical

lian brains (due to tangential expansion of the gray matter with respect to the white matter during growth).^[9] Advances in the methods to synthesize organic and inorganic stimuli-responsive materials,^[10–12] micro-/nanofabrication techniques,^[13] and computational sciences have enabled researchers to apply


Dr. A. M. Abdullah
Department of Mechanical Science and Engineering
University of Illinois at Urbana-Champaign
Urbana, IL 61801, USA
E-mail: arif.md.abdullah@gmail.com

Prof. X. Li
Department of Electrical and Computer Engineering
Materials Research Laboratory
University of Illinois at Urbana-Champaign
Urbana, IL 61801, USA

Prof. P. V. Braun
Department of Materials Science and Engineering
Department of Chemistry
Materials Research Laboratory
Beckman Institute for Advanced Science and Technology
University of Illinois at Urbana-Champaign
Urbana, IL 61801, USA

Prof. J. A. Rogers
Center for Bio-Integrated Electronics
Departments of Materials Science and Engineering
Biomedical Engineering, Chemistry, Mechanical Engineering
Electrical Engineering and Computer Science, and Neurological Surgery
Simpson Querrey Institute for Nano/Biotechnology
McCormick School of Engineering, and Feinberg School of Medicine
Northwestern University
Evanston, IL 60208, USA

Prof. K. J. Hsia
School of Mechanical & Aerospace Engineering
School of Chemical & Biomedical Engineering
Nanyang Technological University
50 Nanyang Avenue, Singapore 63979, Singapore
E-mail: kjhsia@ntu.edu.sg

 The ORCID identification number(s) for the author(s) of this article can be found under <https://doi.org/10.1002/adfm.201909888>.

DOI: 10.1002/adfm.201909888

naturally observed self-folding design principles toward the assembling of smart functional devices such as sensors,^[14] actuators,^[15] robots,^[16–18] grippers,^[19] inductors,^[20] batteries,^[21] photonic crystals,^[22] and solar cells.^[23]

The majority of the self-folded systems rely on a multi-layer architecture where hinges (localized variations in thickness/ material properties) are patterned at discrete locations in order to facilitate out-of-plane bending and subsequent 3D transformation of the 2D structures in response to external stimuli.^[4,10,11,13,19,24] While this particular design paradigm presents an attractive route to realize complex shapes with spatially controllable curvatures, certain aspects make the fabrication and eventually the self-folding behavior of the hinged multi-layer structures challenging. For example, these structures rely on heterogeneous integration of materials (with varying chemical and mechanical properties) along both the in-plane and through-thickness directions for their actuation. Apart from introducing more design constraints, incorporating different materials means increased processing times, stricter fabrication requirements (in terms of equipment, chemical reagents, and pre-/ postprocessing steps), and hence higher costs of production.^[25] Additionally, microfabricated self-folded systems have to overcome additional complexities stemming from stringent mask alignments necessary for appropriate registration between different components and might need extremely fine features (lithographically patterned line width) for achieving the desired curvatures.^[5,12] Mismatches in the properties of the constituent materials might also lead to adhesion, delamination, and fracturing issues during the actuation of the structures.^[24,26] Moreover, the presence of numerous layers and materials will inevitably increase the extent of defects thereby negatively affecting the yield and functional performance of the hinged multilayer self-folded structures.^[1]

In an effort to resolve the above-mentioned problems, here we report the programmable and on-demand generation of complex 3D shapes from hinge-less planar bilayers incorporating Kirigami cuts. Kirigami design principles have previously been incorporated into a diverse class of materials to develop mechanical force actuated functional systems for optics,^[27,28] actuation,^[29] soft robotics,^[30] stretchable electronics,^[31,32] energy harvesting,^[33] reconfigurable metamaterials,^[34–36] building skins,^[37] and graphene-based^[38] applications. Our goal here is to explore how rational introduction of Kirigami cuts enhances the range of shapes achievable with stimuli-responsive bilayers. It is worth mentioning that, although the self-folding behavior of bilayers is often thought to be one involving simple unidirectional bending,^[39] the nature of bilayer morphing strongly depends on its geometric parameters and structural instabilities.^[40–42] We rely on a finite element modeling (FEM)^[43–47] guided approach as the FE models enable us to understand the mechanics behind the bilayer shape transformation behavior and the relationships between initial geometries, applied stimulus, and transformed shapes. We also fabricate millimeter-scaled hinge-less poly(dimethylsiloxane) (PDMS) bilayers with different cross-linking densities (Figure S1, Supporting Information) and transform them into complex 3D configurations such as those representing letters from the Roman alphabet, quasi-axisymmetric flower petal-like structures, and open/closed polyhedral architectures with varying number of faces

(through solvent-induced swelling experiments). We exploit the bilayer morphing to demonstrate optical systems with tunable light transmission and reflection windows. As our computational model is based on the theory of elasticity, which is independent of length scales and material properties, our proposed design principles could be realized with a diverse array of material systems across length scales. Our research would broadly contribute toward the development of smart, shape reconfigurable metamaterials, and self-assembly of mesoscale systems.

2. Result and Discussion

Figure 1a,b shows a set of Kirigami shapes where cuts are introduced from the sides of squares and rectangles. The cuts essentially transform a structure with a single aspect ratio into multiple plate and beam-like geometric units with varying aspect ratios. As shown, a cut on a rectangle (square) with edges W and H (W and W) will result in three geometric units where two rectangles with edges W and $(H-B)/2$ are connected by another rectangle with edges A and B . The aspect ratios of the constituent units and hence their subsequent shape transformation behavior could be tuned by adjusting the cut width. These Kirigami shapes are the basic building blocks of a variety of 3D shapes to be demonstrated in this work. We performed finite element calculations to understand the mismatch strain induced bending behavior of the Kirigami-cut structure as a whole and their individual geometric units (separated from the original structure). The aim was to investigate whether the connections between individual units (abrupt changes in dimensions within the structure where one unit ends and another one starts) would change their behavior and if so to what extent. A representative set of results are shown in Figure S2 (Supporting Information) where the curvature values of the individual constituent units (one short, narrow beam and two longer, wider plates) are compared to those of the original structure at varying levels of mismatch strain (bending). As shown, at low strains, the curvature values throughout the entire structure remain relatively uniform. But at high strains, the narrower region exhibits lower curvatures than the wider ones. In all the cases, individual geometric units matched the behavior of their counterparts within the original structure reasonably well. The curvature variations between geometric units could be attributed to the differences in their aspect ratios. We found that for the same length, the bending curvature is higher for wider structures (Figure S3, Supporting Information) but for the same width, the curvature is independent of the length (Figure S4, Supporting Information). For the same bilayer length, increasing the width gradually shifts the bilayer behavior from a state of plane stress to that of plane strain which eventually results in higher curvatures along the bending direction.^[48] But increasing the length (for the same width) does not cause any such shift in the deformation state along the bending direction and hence the curvature values remain the same.

Figure 1c demonstrates the finite element (FEM) calculations of mismatch strain induced curvature values along the longitudinal axis (Y -direction) for the structures shown in Figure 1a. All the structures bent along their longitudinal axes due to energetic considerations^[42] and the pristine rectangle

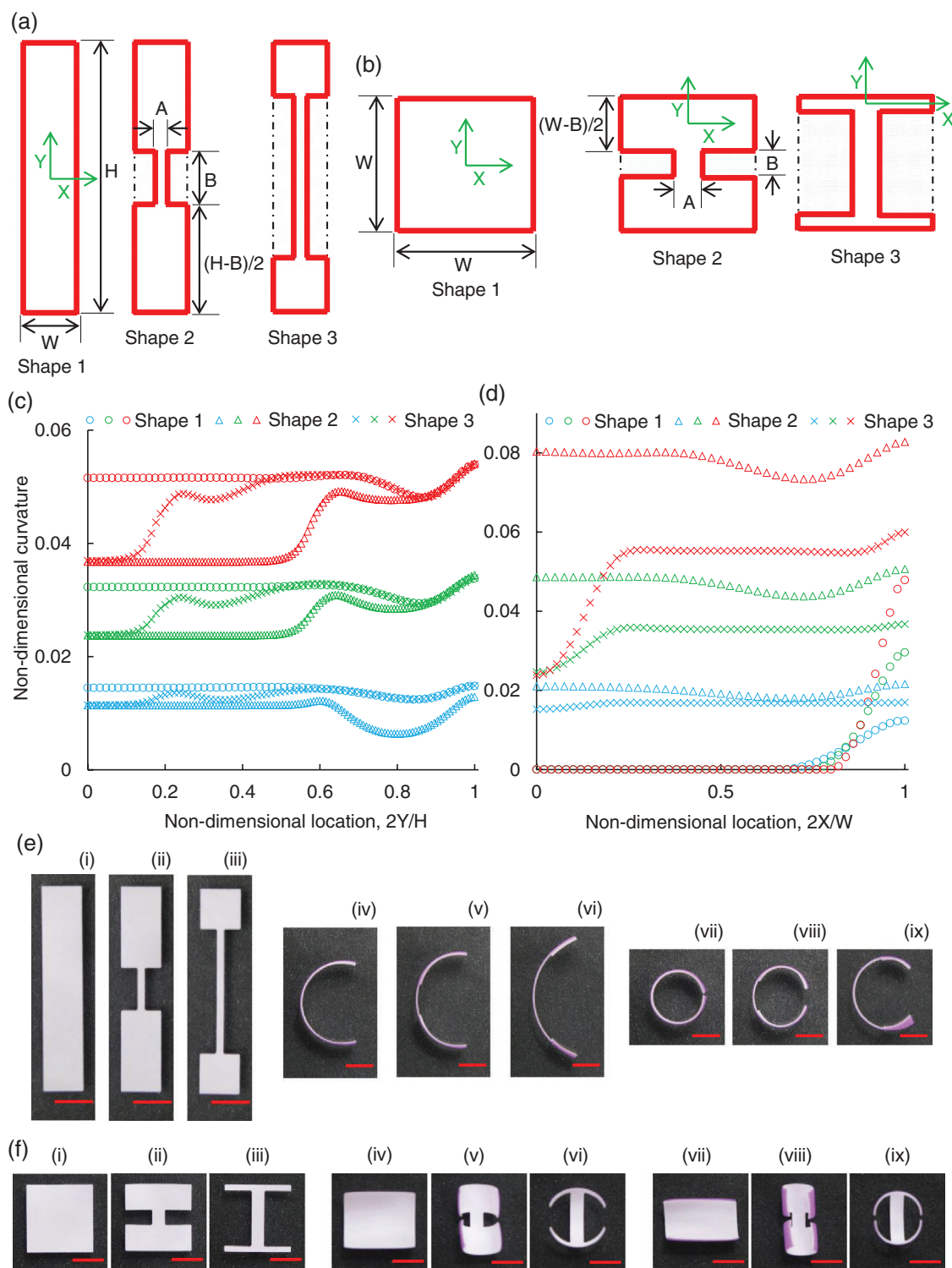


Figure 1. a,b) Rectangles (width W and height H) and squares (arm length W) where cuts are introduced from the sides. The geometric parameters for the Kirigami cuts (width A and height B) are also shown. For a) and the pristine square of b), the origins of the coordinate systems pass through the corresponding geometric centroids. For a) and the pristine square of b), the origins of the coordinate systems pass through the centroids of the units with width $(W - A)$ and height $((W - B)/2)$. c,d) The calculated bending curvature values (at varying mismatch strains) along Y and X directions of the coordinate axes for rectangles and squares shown in (a,b). e,f) The shape transformation behaviors of polymeric bilayers as they swell in organic solvents of varying concentrations (purple layer swells more than the white one). In e,f), (iv) and (vii) are morphed counterparts of (i), (v) and (viii) are morphed counterparts of (ii), and (vi) and (ix) are morphed counterparts of (iii). The scale bars are 5 mm.

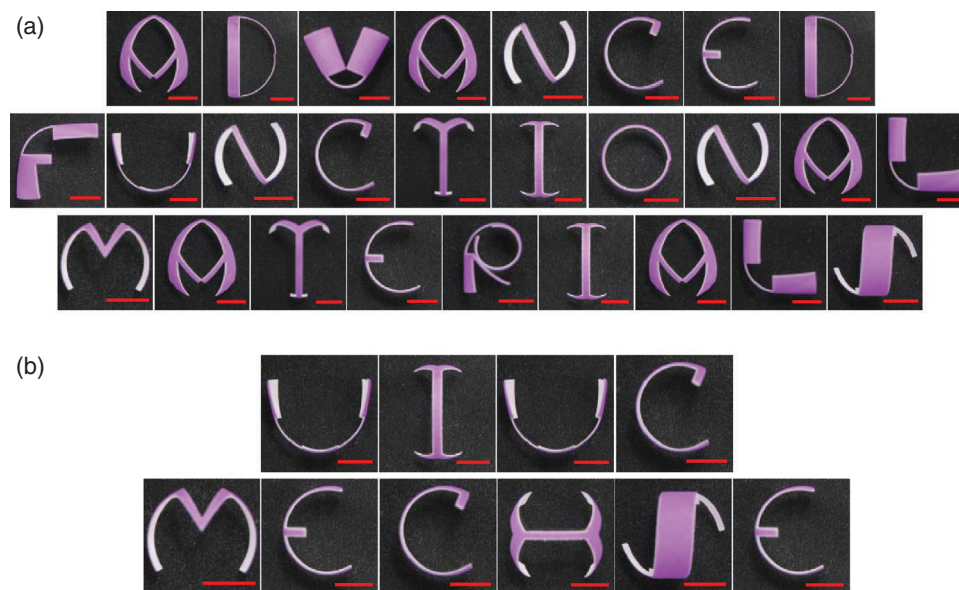


Figure 2. 3D shapes resembling letters from the Roman alphabet are developed through the swelling of Kirigami-cut PDMS bilayers to make up a) ADVANCED FUNCTIONAL MATERIALS and b) UIUC MECHSE (University of Illinois at Urbana-Champaign, Mechanical Science and Engineering). The scale bars are 5 mm.

(shape 1 in Figure 1a), owing to its broader shape at the middle experienced pronounced bending than its counterparts across mismatch strains. For the structures with side cuts (shapes 2 and 3 of Figure 1a), changes in geometric parameters between interconnected units resulted in curvature variations. As the specific locations and extents of the Kirigami cuts (and hence the geometric parameters of the units) are controllable, it is possible to tune the bending curvature values at a particular location for this class of structures. In case of the Kirigami shapes cut from a square (Figure 1b), the geometric units located at the two ends undergo bending along a direction that is perpendicular to that of the pristine square. This occurs as Kirigami cuts change the longitudinal axis directions of the two end-located units. Figure 1d shows the curvature values (along the X-direction) at different mismatch strains for this class of structures calculated using FEM. Near the edges, the pristine squares demonstrated some curvature values as those regions were bent along both the axes. Similar to their rectangular counterparts, the curvature distribution for squares with side cuts depends on their geometric parameters and hence they could be controlled. Figure 1e,f shows the experimental results for the above-mentioned structures as they undergo bending in response to varying mismatch strains. These results illustrate the relationships between geometric parameters, applied stimulus, and the transformed shapes of the Kirigami-cut structures and qualitatively validate our finite element calculations.

The above-mentioned framework presents a unique opportunity for on-demand shape reconfiguration of Kirigami-cut, 2D bilayers into complex 3D shapes. Several demonstrations are shown in Figure 2 where letters from the Roman alphabet are realized through the swelling of PDMS bilayers to form the words ADVANCED FUNCTIONAL MATERIALS, UIUC (University of Illinois at Urbana-Champaign), and MECHSE (Mechanical Science and Engineering). The planar bilayer designs, their

gradual shape transformation behavior with varying mismatch strains, and corresponding finite element calculations are included in the supplementary material (Figures S5–S19, Supporting Information). As demonstrated, mechanistic principles can be employed to design Kirigami-cut bilayers where the interconnected geometric units vary both in dimensions and axial directions. Such differences are responsible for the spatial variations in their bending directions and curvature values. Using the same principle, other classes of complex 3D shapes could also be realized as the strategic generation and subsequent modification of the geometric units depend on the rational incorporation of Kirigami cuts within bilayered rectangles/ squares. Development of a comprehensive optimization scheme could also be done to solve the inverse problem of identifying the 2D bilayer design parameters and required extent of the external stimuli for given 3D shapes.

Figure 3a shows the second group of structures where radial cuts are introduced within pristine squares. The cuts start from a circle at the center of a square and extend to the corners. For a square of side length L , these shapes could be defined by the radii of the circular mid-section R and cut width α (angles subtended by the cuts at the centroid of the square). We performed finite element computations to understand the stimuli-responsive shape transformation behavior of these structures and observed bifurcation of equilibrium shapes. Bifurcation is a structural instability mechanism solely arising from the nonlinear geometric behavior of thin shell structures that eventually minimizes the mid-section stretching at high mismatch strains.^[40,41,49] In our case, the squares with Kirigami cuts transitioned from quasi-axisymmetric doubly curved shapes to asymmetric singly curved ones at critical strains. The effects of their initial shapes on bifurcation strains are shown in Figure 3b. Shapes with larger R bifurcate at lower mismatch strains while showing minor dependence on the cut width.

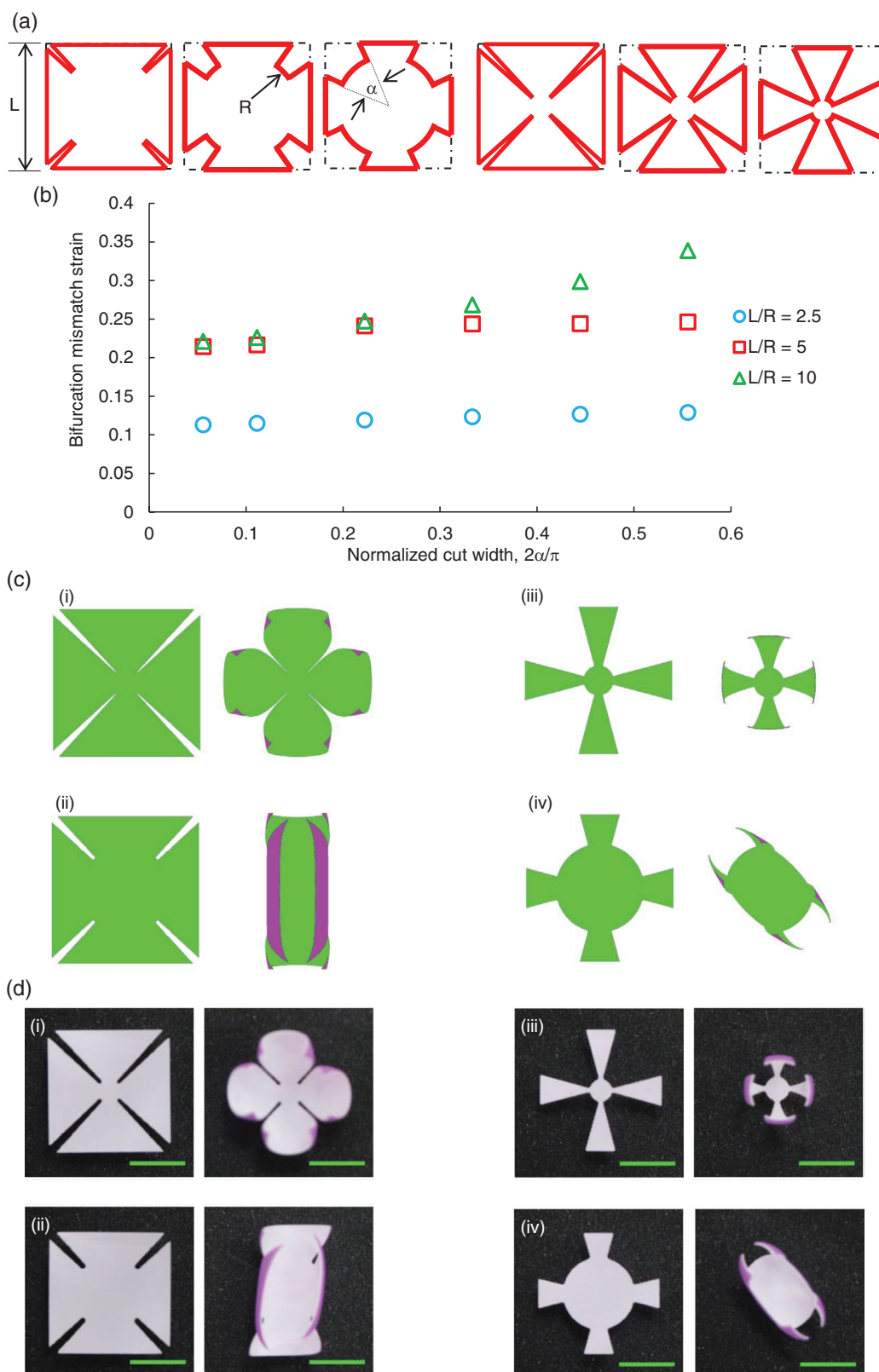


Figure 3. a) The geometric parameters (arm length L , mid-section radius R , and cut width α) for squares with radial Kirigami cuts. b) Dependence of the bifurcation mismatch strains on the geometry of the Kirigami-cut squares. Computational findings on the shape transformation behavior of these structures are presented in (c). Experimental demonstrations where Kirigami-cut PDMS bilayers assume prebifurcated/postbifurcated configurations after swelling in organic solvents are included in (d). The scale bars for (d) are 5 mm.

When the mid-section circle radius R is small, bifurcation occurs at higher mismatch strains as the radial cuts become bigger. The effects of the geometric parameters on curvature–mismatch strain relationships are demonstrated in Figure S20 (Supporting Information). As shown, prior to bifurcation the extent of out-of-plane deformation (hence curvature) remains the same along all the directions but at the post-bifurcated state, cylindrical configurations with preferred bending directions emerge. The computational predictions and experimental results for the shape transformation behavior of this class of structures are shown in Figure 3c,d (also Videos S1 and S2, Supporting Information). Of the four structures, (i) and (iii) have smaller circular mid-sections than their counterparts shown in (ii) and (iv) (Figure 3c,d). At the same value of mismatch strain, structures with large mid-sections bifurcated into singly curved configurations while the ones with small mid-sections retained their quasi-axisymmetric prebifurcated shapes. For prebifurcated structures, we observed either a cage-like shape (large cuts—(iii) in (Figure 3c,d) or a flower petal-like shape (small cuts—(i) in (Figure 3c,d) where free corners of individual triangular plates undergo out-of-plane bending as they come toward each other. It is to be mentioned that the experimental images demonstrated here were captured from the top. Side views of deformed 3D structures (obtained through mismatch strain driven bending of bilayers) were reported elsewhere.^[41]

For squares with radial Kirigami cuts, we also investigated the class of structures where the cuts pass through the edges instead of corners (Figure S21, Supporting Information). These structures also demonstrated the occurrence of bifurcation where the critical strains were dependent on the mid-section sizes and cut widths. The effects of geometric parameters on the transformed configurations (i.e., prebifurcated axisymmetric or postbifurcated asymmetric ones) at a given mismatch strain are also evident. The variations in the bifurcation behavior of different squares with radial Kirigami cuts arise from their differences in the geometric parameters as L/R ratios governed the extent to which the Kirigami sheets experienced bending and stretching. Within our computational scheme, we ensured that the elements used in our finite element mesh were significantly smaller than the geometric parameters of the analyzed structure. This is necessary for accurately capturing the deformation behavior of the Kirigami sheets. If the Kirigami sheets approach size scales where the discrete structure of the matter dominates and the classical elasticity theory is not applicable anymore (tens of nanometer),^[50] molecular dynamic simulations would be necessary (instead of finite element modeling) to understand the deformation behavior.

A few of the shapes reported in this work have some similarities with swellaible multilayer configurations reported in the literature.^[51,52] However, our work differs in terms of geometric parameters and patterning requirements. We consider square and rectangular bilayers with side/radial Kirigami cuts. Due to their plate-like configurations, these structures undergo a combination of in-plane stretching and out-of-plane bending (instead of unidirectional bending as observed in beam-like structures). Although the occurrence of bifurcation eventually leads to the bending of the Kirigami-cut sheets at higher strains, the selection of plate-like structures offers additional opportunities to tune the bilayer shapes at varying mismatch strains

(quasi-axisymmetric doubly curved and asymmetric singly curved as stated earlier). Also, our structures did not have any in-plane patterned hinges (localized variations in thickness/material properties). Due to this reason, the fabrication of our bilayers is straightforward and the actuation protocol is simple.

We further explored possible applications for the above-mentioned structures as tunable optical transmission and reflection systems.^[27,53,54] For these experiments, we incorporated fluorescence nanoparticles within the PDMS matrix and performed fluorescence microscopy (at varying mismatch strains) to compare luminescence profiles, as demonstrated in Figure 4. A high luminescence value refers to an elevated level of optical reflection while a low luminescence value means that the particular sample is primarily transmitting the incident light. Figure 4a shows a geometry with large cut widths at low and high mismatch strains with corresponding luminescence profiles along different directions. As the structure undergoes out-of-plane bending, changes in its reflective behaviors are evident as the peak luminescence value is reached in a much more gradual manner (Figure 4a-iv) than that of its counterpart where the deformation is negligible (Figure 4a-iii). The sizes of the reflection window along the two orthogonal directions remained the same when compared to each other (low mismatch strains—green and red lines in Figure 4a-iii, high mismatch strains—blue and yellow lines in Figure 4a-iv) as bifurcation is yet to occur for this particular geometry. However, the optical reflection window shrinks (yellow line in Figure 4a-ii) from its original state (red line in Figure 4a-i) as the projected edge to edge length decreases at high mismatch strains (Figure 4a-v). As shown in Figure 4b, bifurcation is observed when the cut widths are small (while the remaining geometric parameters remain unchanged) and hence it is possible to achieve different reflective behaviors along the two orthogonal directions at high mismatch strains (blue and yellow lines in Figure 4b-iii).

Bifurcation also changes the optical behavior along the diagonal direction in a significant manner as demonstrated by the presence of multiple peaks and valleys on the luminescence profile (Figure 4b-iv). Compared to its original shape (red line in Figure 4b-i), the plateau at the middle is bigger due to stretching of the mid-section (green line in Figure 4b-ii). The overall size of the optical reflection window becomes bigger as the neighboring units come toward each other and where their corners meet, optical reflection occurs (Figure 4b-iv). The peaks and the valleys on each side of the plateau emerge due to the overlapping of the edges (variations in out-of-plane deformation) and optical transmission through the pre-existing gaps between the units. Complex optical reflection windows (with multiple peaks and valleys) could also be generated from the shape transformation behavior of structures where the Kirigami cuts pass through edges instead of corners (Figure 4c). At the postbifurcated state, a portion of the strongly cross-linked layer could be seen through the cuts. Due to variations in out-of-plane deformation, this layer demonstrates different optical transmission characteristics as shown in the luminescence profile. The optical tunabilities of the proposed systems could be enhanced further through the incorporation of other types of Kirigami cuts and/or fluorescence species (with very different excitation frequencies). We would like to mention that, unlike traditional optical metamaterials, the structures demonstrated

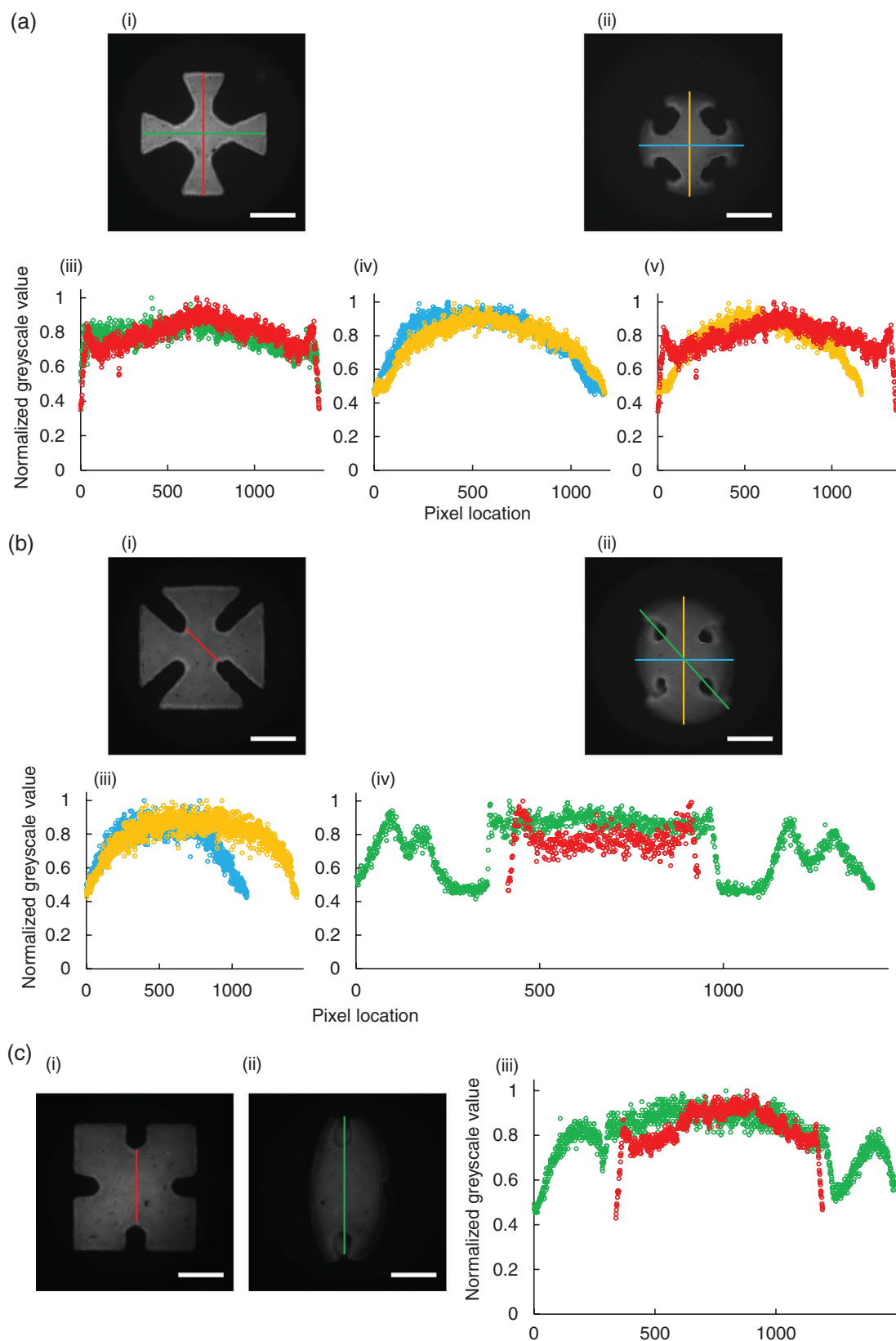


Figure 4. Demonstration of Kirigami-cut squares as optical metamaterials. The plotted luminescence profiles are along the lines drawn on the fluorescent images. a) The shrinking of the optical reflection windows (similar along the two orthogonal directions) prior to bifurcation. b) The selective shrinking (along one direction) and tuning of both the optical transmission and reflection windows (along the diagonal direction) after bifurcation. c) The broadening of the optical reflection window through variations in out-of-plane displacements of different portions within a bilayer. Scale bars are 1 mm.

in this work are bigger than the wavelength of the transmitted/reflected light. However, our proposed design principles could be realized at smaller length scales (hundreds of nanometers) to achieve tunable optical properties from engineered systems that transform their shapes in response to external stimuli.

A combination of radial and side cuts could be used to develop other classes of complex 3D shapes of functional interest in an on-demand manner. Polyhedral geometries are one such family of structures with demonstrated applications as small scale containers for chemical delivery, sensors, metamaterials, 3D graphene-based devices, and microfluidic systems.^[55–59] Motivated by the hierarchical assembly of small-scale biological materials, origami-like self-folding protocols have been developed where planar sheets with localized hinges undergo stimuli-responsive bending to transform into polyhedra with multiple faces. In this article, we show the possibility of realizing polyhedral shapes from Kirigami-cut bilayers that do not require spatially patterned hinges for their shape morphing. The curvature variations in hinged systems (higher curvature near the hinges and lower/zero curvature away from the hinges) stem from localized variations in thickness and/or material properties introduced through lithographic patterning. Modifying the above-mentioned structural parameters results in out-of-plane bending stiffness variations, which could also be achieved through the alteration of in-plane geometric characteristics.

In Figure 5a–d, pristine triangles and squares of varying sizes are modified with Kirigami cuts to create geometries consisting of multiple triangular (equilateral) and square-shaped units connected by narrower links. The in-plane geometric parameters for the Kirigami-cut square are shown in Figure S22 (Supporting Information) where each of the five plate-like units has arm lengths “ L ” and each of the four links have arm lengths “ H ” ($H < L$). When the bilayer is thin (Figure S23, Supporting Information), each of the five square-shaped plates assumes prebifurcated shapes with minimal out-of-plane bending (considerable in-plane stretching) at low mismatch strains. These units eventually bifurcate at high strains as confirmed by the curvature contours. The four links, however, undergo unidirectional bending across all the mismatch strains owing to their boundary conditions (two edges free and two others are connected to two different units). The behavioral difference between the two types of units is responsible for the shape at high strains where the bending curvature is higher along the X-axis than that along the Y-axis (Video S3, Supporting Information). When the bilayer is thick, the four links again experience unidirectional bending but the five plates maintain their pre-bifurcated shapes up to high strains. This leads to the development of a five-faced open box-like shape where the five bigger units of the planar bilayer are curved to the same extent along both the co-ordinate axes (Figure S24 and Video S4, Supporting Information).

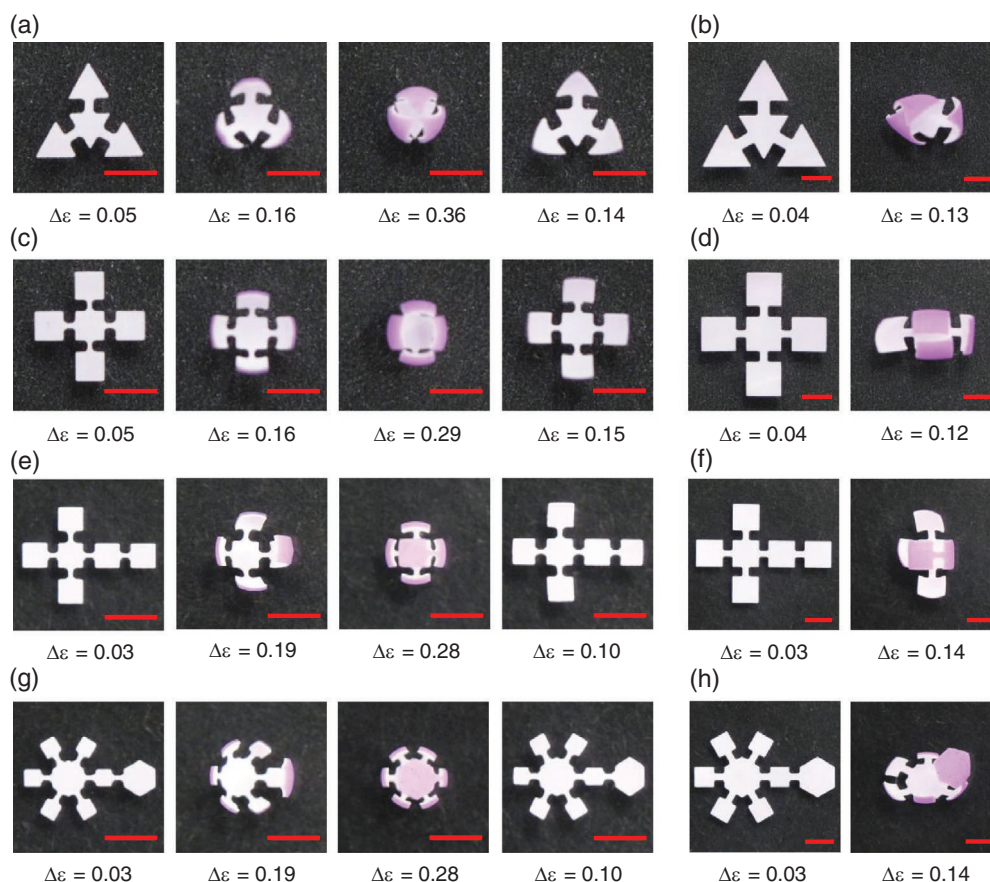


Figure 5. Morphing of Kirigami-cut bilayers into polyhedral geometries such as a) tetrahedron, b) open cube with five faces, c) cube, and d) hexagonal prism. For these four demonstrations, gradual shape transformations of the bilayers are shown at increasing and decreasing mismatch strains. Bifurcated counterparts of a,c,e,g) are shown in b,d,f,h). Scale bars are 3 mm.

Generation of polyhedral shapes is governed by the occurrence of bifurcation. In Figure S25 (Supporting Information), we show computational results elucidating how bifurcation mismatch strains depend on the geometric parameters of the Kirigami-cut square. For a constant bilayer thickness, bifurcation occurs at higher strains for higher values of L/H . When H is low, the links do not affect the behavior of the plates. As the links get bigger, their unidirectional bending tends to impact the morphing behavior of the plates to a greater extent (due to enhanced connections) and hence bifurcation occurs earlier. For constant values of H and L , thinner bilayers bifurcate at lower strains owing to their intrinsic compliance for bending and vice versa. Generation of pyramids/five-faced open boxes (prebifurcated) or postbifurcated shapes from Kirigami-cut bilayers is rationalized through the above-mentioned design principles. Building upon them, we also report complex polyhedral shapes such as hexahedron (cube—six square-shaped faces) and octahedron (hexagonal prism—two hexagonal-shaped and six square-shaped faces) with their bifurcated counterparts as shown in Figure 5e–h and Videos S5 and S6 (Supporting Information). For the fabrication functional polyhedra, the individual faces of the bilayer might need appropriate patterning before self-folding. In those cases, the design guidelines developed in this work would still be applicable as they are independent of particular processing and/or material characteristics.

In this work, our choice of the material-solvent system was based on our prior research expertise and experimental convenience. As our computational model is independent of material selection, the design principles reported here would be applicable to other stimuli-responsive material systems. Hence, polymers and hydrogels responsive to functionally relevant stimuli such as heat (liquid-crystal elastomer (LCE)),^[60] shape-memory polymer,^[61] and pNIPAM^[62], chemical/solvent diffusion (poly(3,4-ethylenedioxythiophene):polystyrene sulfonate (PEDOT:PSS))^[63] and poly(ethylene glycol) diacrylate^[64], light (shape-memory polymer^[65] and graphene oxide/ polypeptide composite^[66]), biochemical enzymes (gelatin and carboxymethylcellulose^[67]), salt concentration (poly(methacryloxyethyltrimethylammonium chloride))^[68], pH (acrylic acid and 2-(dimethylamino) ethyl methacrylate^[69]), and magnetic fields (polypyrrole embedded with Ni/Au^[70] and PDMS embedded with Fe^[49]) could be used to self-assemble bilayered Kirigami sheets. As a possible application of our work, we demonstrated a dynamically tunable optical system realized from self-assembled Kirigami sheets. However, tetherless and on-demand shape reconfiguration behavior of Kirigami structures could also be used to design smart functional entities such as sensors, actuators, drug delivery devices, tissue engineering scaffolds, robots, and energy harvesting systems.

3. Conclusion

Our work demonstrates the possibility of achieving complex 3D shapes in a programmable and on-demand manner from freestanding, hingeless, 2D bilayers of uniform thickness. Our approach involves the incorporation of Kirigami cuts within the geometry of self-folding bilayers where one layer isotropically

expands with respect to the other in response to an external stimulus. We develop nonlinear finite element models to identify the relationships between initial bilayer geometry, applied stimulus, and transformed configurations. We verify the mechanistic understandings through swelling experiments of PDMS bilayers with varying cross-linking densities and generate intricate shapes such as letters from the Roman alphabet and open/closed polyhedral architectures. We also present a dynamically tunable optical system whose light transmission and reflection behaviors could be controlled through bilayer shape transformation. As the proposed design principles rely on a computational framework which is independent of length scales and material properties, our work could contribute toward the development of smart functional systems for sensing, actuation, optics, electronics, drug delivery, and tissue engineering applications.

4. Experimental Section

Finite Element Analysis: The commercially available finite element analysis package ABAQUS^[71] for understanding the mechanics of the stimulus-responsive shape transformation behavior of Kirigami-cut bilayers was used. Following an already established protocol,^[40,43,72–74] the mismatch strain-driven bilayer morphing was modeled as an equivalent thermal expansion problem where one layer expands with respect to the other in response to a hypothetical temperature. In our computations, 4-node general purpose shell elements with through-thickness variation in material properties (the element size was determined from separate mesh refinement studies) and appropriate boundary conditions were used. While simulating the bifurcation behavior, small imperfections^[40,41,49] were incorporated for reliably capturing the bilayer deformation beyond critical strains. Hyperelastic material properties (bulk and shear moduli are 962 and 0.18 MPa for the weakly cross-linked layer and 1214.8 and 32.2 MPa for the densely cross-linked layer) were used in our model. As the swelling of PDMS in organic solvents results in polymeric gels with nonlinear material properties,^[75,76] our approach enabled to develop qualitative predictions of the bilayer morphing behavior applicable to other stimulus-responsive material systems in general.

Experimental Protocol: Polydimethylsiloxane (Dow Corning Sylgard 184—Ellsworth Adhesives), silicone pigments (Cirius Silicone pigments—Dick Blick Art Materials), and fluorescent dyes (Fluorescein sodium salt—Sigma-Aldrich and Alexa Fluor 594—Thermo Fisher Scientific) were used to fabricate two sets of bilayer samples where the first set was used for general shape transformation experiments (Figures 1, 2, 3, and 5) and the second set was used for optical metamaterial demonstrations (Figure 4). In general, we started by developing the mixture for the densely cross-linked layer (1 part white pigment: 2 parts base: 8 parts crosslinker for the first set and 1 part white pigment: 2 parts base: 8 parts crosslinker: 1.1 parts diluted Fluorescein for the second set) which is spin-coated on pre-cleaned glass slides and partially cured in an oven for 30 min at 90 °C. Then the mixture for the weakly cross-linked layer (1 part purple pigment: 0.48 parts base: 9.52 parts crosslinker for the first set and 1 part purple pigment: 0.48 parts base: 9.52 parts crosslinker: 1.1 parts diluted Alexa Fluor for the second set) was developed, which is spin-coated on top of the partially cured layer and the entire bilayer is cured for 60 min at 70 °C. The spin-coating was done for 30 s at 720 rpm and at 1030 rpm for the first and second set of samples. Bilayers of different shapes were laser-cut from the glass-slides once they reached room temperature after curing. A previously reported protocol was followed to perform the bilayer shape transforming experiments in solvent mixtures of 1-propanol and xylene (Fisher scientific).^[41,49] ImageJ^[77] was used for postprocessing the figure presented in this paper.

Supporting Information

Supporting Information is available from the Wiley Online Library or from the author.

Acknowledgements

A.M.A. acknowledges support from the Food Machinery Corporation (FMC) Educational Fund Fellowship and the Graduate College Dissertation Completion Fellowship through the University of Illinois at Urbana-Champaign. The authors acknowledge partial support from the U.S. Department of Energy, Office of Science, Basic Energy Sciences, under Award No. DE-FG02-07ER46471. K.J.H. acknowledges partial support from Nanyang Technological University, Singapore, and from the Carnegie Mellon University.

Conflict of Interest

The authors declare no conflict of interest.

Keywords

metamaterials, self-assembly, stimuli responsive

Received: November 27, 2019
Published online: February 16, 2020

- [1] M. Boncheva, G. M. Whitesides, *MRS Bull.* **2005**, *30*, 736.
- [2] G. M. Whitesides, M. Boncheva, *Proc. Natl. Acad. Sci. USA* **2002**, *99*, 4769.
- [3] B. Alberts, A. Johnson, J. Lewis, M. Raff, K. Roberts, P. Walter, *Molecular Biology of the Cell*, Garland Science, Taylor & Francis Group, New York, NY **2002**.
- [4] T. G. Leong, A. M. Zarafshar, D. H. Gracias, *Small* **2010**, *6*, 792.
- [5] J. Rogers, Y. Huang, O. G. Schmidt, D. H. Gracias, *MRS Bull.* **2016**, *41*, 123.
- [6] J. M. Skotheim, *Science* **2005**, *308*, 1308.
- [7] Y. Forterre, *J. Exp. Bot.* **2013**, *64*, 4745.
- [8] E. Cerda, L. Mahadevan, *Phys. Rev. Lett.* **2003**, *90*, 074302.
- [9] T. Tallinen, J. Y. Chung, J. S. Biggins, L. Mahadevan, *Proc. Natl. Acad. Sci. USA* **2014**, *111*, 12667.
- [10] J. S. Randhawa, K. E. Laffin, N. Seelam, D. H. Gracias, *Adv. Funct. Mater.* **2011**, *21*, 2395.
- [11] L. Ionov, *Adv. Funct. Mater.* **2013**, *23*, 4555.
- [12] L. Ionov, *Soft Matter* **2011**, *7*, 6786.
- [13] Y. Zhang, F. Zhang, Z. Yan, Q. Ma, X. Li, Y. Huang, J. A. Rogers, *Nat. Rev. Mater.* **2017**, *2*, 17019.
- [14] J. H. Cho, S. Hu, D. H. Gracias, *Appl. Phys. Lett.* **2008**, *93*, 043505.
- [15] L. Hines, K. Petersen, G. Z. Lum, M. Sitti, *Adv. Mater.* **2017**, *29*, 1603483.
- [16] W. Hu, G. Z. Lum, M. Mastrangeli, M. Sitti, *Nature* **2018**, *554*, 81.
- [17] S. Felton, M. Tolley, E. Demaine, D. Rus, R. Wood, *Science* **2014**, *345*, 644.
- [18] S. Coyle, C. Majidi, P. LeDuc, K. J. Hsia, *Extreme Mech. Lett.* **2018**, *22*, 51.
- [19] E. Gultepe, J. S. Randhawa, S. Kadam, S. Yamanaka, F. M. Selaru, E. J. Shin, A. N. Kalloo, D. H. Gracias, *Adv. Mater.* **2013**, *25*, 514.
- [20] W. Huang, X. Yu, P. Froeter, R. Xu, P. Ferreira, X. Li, *Nano Lett.* **2012**, *12*, 6283.
- [21] W. Si, I. Mönch, C. Yan, J. Deng, S. Li, G. Lin, L. Han, Y. Mei, O. G. Schmidt, *Adv. Mater.* **2014**, *26*, 7973.
- [22] S. Giudicatti, S. M. Marz, L. Soler, A. Madani, M. R. Jorgensen, S. Sanchez, O. G. Schmidt, *J. Mater. Chem. C* **2014**, *2*, 5892.
- [23] X. Guo, H. Li, B. Yeop Ahn, E. B. Duoss, K. J. Hsia, J. A. Lewis, R. G. Nuzzo, *Proc. Natl. Acad. Sci. USA* **2009**, *106*, 20149.
- [24] V. B. Shenoy, D. H. Gracias, *MRS Bull.* **2012**, *37*, 847.
- [25] M. J. Madou, *Fundamentals of Microfabrication and Nanotechnology*, CRC Press, Boca Raton, FL **2012**.
- [26] D. H. Gracias, *Curr. Opin. Chem. Eng.* **2013**, *2*, 112.
- [27] W. Wang, C. Li, H. Rodrigue, F. Yuan, M.-W. Han, M. Cho, S.-H. Ahn, *Adv. Funct. Mater.* **2017**, *27*, 1604214.
- [28] Y. Zhang, Z. Yan, K. Nan, D. Xiao, Y. Liu, H. Luan, H. Fu, X. Wang, Q. Yang, J. Wang, W. Ren, H. Si, F. Liu, L. Yang, H. Li, J. Wang, X. Guo, H. Luo, L. Wang, Y. Huang, J. A. Rogers, *Proc. Natl. Acad. Sci. USA* **2015**, *112*, 11757.
- [29] M. A. Dias, M. P. McCarron, D. Rayneau-Kirkhope, P. Z. Hanakata, D. K. Campbell, H. S. Park, D. P. Holmes, *Soft Matter* **2017**, *13*, 9087.
- [30] A. Rafsanjani, Y. Zhang, B. Liu, S. M. Rubinstein, K. Bertoldi, *Sci. Rob.* **2018**, *3*, eaar7555.
- [31] C. Wu, X. Wang, L. Lin, H. Guo, Z. L. Wang, *ACS Nano* **2016**, *10*, 4652.
- [32] T. C. Shyu, P. F. Damasceno, P. M. Dodd, A. Lamoureux, L. Xu, M. Shlian, M. Shtein, S. C. Glotzer, N. A. Kotov, *Nat. Mater.* **2015**, *14*, 785.
- [33] A. Lamoureux, K. Lee, M. Shlian, S. R. Forrest, M. Shtein, *Nat. Commun.* **2015**, *6*, 8092.
- [34] Y. Cho, J.-H. Shin, A. Costa, T. A. Kim, V. Kunin, J. Li, S. Y. Lee, S. Yang, H. N. Han, I.-S. Choi, D. J. Srolovitz, *Proc. Natl. Acad. Sci. USA* **2014**, *111*, 17390.
- [35] Y. Tang, G. Lin, L. Han, S. Qiu, S. Yang, J. Yin, *Adv. Mater.* **2015**, *27*, 7181.
- [36] Y. Tang, J. Yin, *Extreme Mech. Lett.* **2017**, *12*, 77.
- [37] Y. Tang, G. Lin, S. Yang, Y. K. Yi, R. D. Kamien, J. Yin, *Adv. Mater.* **2017**, *29*, 1604262.
- [38] M. K. Bles, A. W. Barnard, P. A. Rose, S. P. Roberts, K. L. McGill, P. Y. Huang, A. R. Ruyack, J. W. Kevek, B. Kobrin, D. A. Muller, P. L. McEuen, *Nature* **2015**, *524*, 204.
- [39] S. Timoshenko, *J. Opt. Soc. Am.* **1925**, *11*, 233.
- [40] L. B. Freund, *J. Mech. Phys. Solids* **2000**, *48*, 1159.
- [41] A. M. Abdullah, P. V. Braun, K. J. Hsia, *Appl. Phys. Lett.* **2017**, *111*, 104101.
- [42] S. Alben, B. Balakrishnan, E. Smela, *Nano Lett.* **2011**, *11*, 2280.
- [43] A. M. Abdullah, P. V. Braun, K. J. Hsia, *Soft Matter* **2016**, *12*, 6184.
- [44] K. Bertoldi, P. M. Reis, S. Willshaw, T. Mullin, *Adv. Mater.* **2010**, *22*, 361.
- [45] K. Nan, H. Luan, Z. Yan, X. Ning, Y. Wang, A. Wang, J. Wang, M. Han, M. Chang, K. Li, Y. Zhang, W. Huang, Y. Xue, Y. Huang, Y. Zhang, J. A. Rogers, *Adv. Funct. Mater.* **2017**, *27*, 1604281.
- [46] C. Huang, D. Quinn, S. Suresh, K. J. Hsia, *Proc. Natl. Acad. Sci. USA* **2018**, *115*, 70.
- [47] C. Huang, Z. Wang, D. Quinn, S. Suresh, K. J. Hsia, *Proc. Natl. Acad. Sci. USA* **2018**, *115*, 12359.
- [48] G. P. Nikishkov, *J. Appl. Phys.* **2003**, *94*, 5333.
- [49] A. M. Abdullah, X. Li, P. V. Braun, J. A. Rogers, K. J. Hsia, *Adv. Mater.* **2018**, *30*, 1801669.
- [50] R. Maranganti, P. Sharma, *Phys. Rev. Lett.* **2007**, *98*, 195504.
- [51] Y. Ma, Y. Zhang, B. Wu, W. Sun, Z. Li, J. Sun, *Angew. Chem., Int. Ed.* **2011**, *50*, 6254.
- [52] C. M. Andres, J. Zhu, T. Shyu, C. Flynn, N. A. Kotov, *Langmuir* **2014**, *30*, 5378.
- [53] L. Xu, X. Wang, Y. Kim, T. C. Shyu, J. Lyu, N. A. Kotov, *ACS Nano* **2016**, *10*, 6156.
- [54] J.-H. Cho, M. D. Keung, N. Verellen, L. Lagae, V. V. Moshchalkov, P. Van Dorpe, D. H. Gracias, *Small* **2011**, *7*, 1943.

- [55] H. Ye, C. L. Randall, T. G. Leong, D. A. Slanac, E. K. Call, D. H. Gracias, *Angew. Chem., Int. Ed.* **2007**, *46*, 4991.
- [56] K. Agarwal, C. Liu, D. Joung, H.-R. Park, S.-H. Oh, J.-H. Cho, *Sci. Rep.* **2017**, *7*, 2680.
- [57] K. Agarwal, C. Liu, D. Joung, H.-R. Park, J. Jeong, D.-S. Kim, J.-H. Cho, *ACS Photonics* **2017**, *4*, 2436.
- [58] D. Joung, T. Gu, J.-H. Cho, *ACS Nano* **2016**, *10*, 9586.
- [59] J.-R. Park, D. A. Slanac, T. G. Leong, H. Ye, D. B. Nelson, D. H. Gracias, *J. Microelectromech. Syst.* **2008**, *17*, 265.
- [60] T. H. Ware, M. E. McConney, J. J. Wie, V. P. Tondiglia, T. J. White, *Science* **2015**, *347*, 982.
- [61] W. Voit, T. Ware, R. R. Dasari, P. Smith, L. Danz, D. Simon, S. Barlow, S. R. Marder, K. Gall, *Adv. Funct. Mater.* **2010**, *20*, 162.
- [62] G. Stoychev, N. Puretskiy, L. Ionov, *Soft Matter* **2011**, *7*, 3277.
- [63] S. Taccola, F. Greco, E. Sinibaldi, A. Mondini, B. Mazzolai, V. Mattoli, *Adv. Mater.* **2015**, *27*, 1668.
- [64] H. R. Kwag, J. V. Serbo, P. Korangath, S. Sukumar, L. H. Romer, D. H. Gracias, *Tissue Eng., Part C* **2016**, *22*, 398.
- [65] Y. Yu, T. Ikeda, *Macromol. Chem. Phys.* **2005**, *206*, 1705.
- [66] E. Wang, M. S. Desai, S.-W. Lee, *Nano Lett.* **2013**, *13*, 2826.
- [67] N. Bassik, A. Brafman, A. M. Zarafshar, M. Jamal, D. Luvsanjav, F. M. Selaru, D. H. Gracias, *J. Am. Chem. Soc.* **2010**, *132*, 16314.
- [68] T. S. Kelby, M. Wang, W. T. S. Huck, *Adv. Funct. Mater.* **2011**, *21*, 652.
- [69] L. Dong, A. K. Agarwal, D. J. Beebe, H. Jiang, *Nature* **2006**, *442*, 551.
- [70] B. Jang, E. Gutman, N. Stucki, B. F. Seitz, P. D. Wendel-García, T. Newton, J. Pokki, O. Ergeneman, S. Pané, Y. Or, B. J. Nelson, *Nano Lett.* **2015**, *15*, 4829.
- [71] Abaqus, Dassault Systemes, Providence, RI, USA **2014**, <http://dsk.ippt.pan.pl/docs/abaqus/v6.13/index.html> (accessed: May 2019).
- [72] A. M. Abdullah, K. Nan, J. A. Rogers, K. J. Hsia, *Extreme Mech. Lett.* **2016**, *7*, 34.
- [73] H. Yang, F. Fan, W. Liang, X. Guo, T. Zhu, S. Zhang, *J. Mech. Phys. Solids* **2014**, *70*, 349.
- [74] G. Stoychev, S. Turcaud, J. W. C. Dunlop, L. Ionov, *Adv. Funct. Mater.* **2013**, *23*, 2295.
- [75] W. Hong, X. Zhao, J. Zhou, Z. Suo, *J. Mech. Phys. Solids* **2008**, *56*, 1779.
- [76] W. Hong, Z. Liu, Z. Suo, *Int. J. Solids Struct.* **2009**, *46*, 3282.
- [77] C. A. Schneider, W. S. Rasband, K. W. Eliceiri, *Nat. Methods* **2012**, *9*, 671.